Modelling Line and Edge Features Using Higher-Order Riesz Transforms*

Ross Marchant[1,2] and Paul Jackway[2]

[1] James Cook University
[2] CSIRO Computational Informatics

Abstract. The 2D-complex Riesz transform is an extension of the Hilbert transform to images. It can be used to model local image structure as a superposition of sinusoids, and to construct 2D steerable wavelets. In this paper we propose to model local image structure as the superposition of a 2D steerable wavelet at multiple amplitudes and orientations. These parameters are estimated by applying recent developments in super-resolution theory. Using 2D steerable wavelets corresponding to line or edge segments then allows for the underlying structure of image features such as junctions and edges to be determined.

Keywords: Riesz transform, 2D steerable filter, super-resolution, semi-definite program, local feature analysis.

1 Introduction

Low-level image features arise from interesting structures such as lines, edges, corners and junctions. Detection, classification and parametrisation of such features is a useful first step in the image analysis pipeline, providing input for higher-level pattern recognition. One approach is to project the local image patch onto a particular signal model. The model may be as simple as edge detection, or a more complex description with geometric information, e.g. [1]. The monogenic signal [2] locally models an image as an oriented sinusoid with a certain amplitude, phase and orientation, using the 1st order Riesz transform (RT). This representation is useful as amplitude encodes feature strength and phase encodes feature type, e.g. line or edge. Higher-order RTs are used for more complex signal models in [3] [4] and [5], and recent research has shown RTs can be used to construct 2D steerable wavelets [6], [7].

In this paper we propose to extend this work to model local signal structure as the superposition of a particular 2D steerable wavelet at multiple amplitudes and orientations. This is an inverse problem where these parameters must be optimised such that the model describes as much of the signal as possible. Our novel approach is to use the theory of super-resolution of spike trains via semi-definite programming [8], [9] to solve for the wavelet parameters. The choice of wavelet

* The first author is supported by JCU and CSIRO scholarships. This research is part of the CSIRO Transformational Biology Capability Platform.

J. Blanc-Talon et al. (Eds.): ACIVS 2013, LNCS 8192, pp. 438–449, 2013.
© Springer International Publishing Switzerland 2013

depends on the feature of interest. For example, if a wavelet corresponding to a line segment or wedge segment is used, then the amplitude and orientation of individual line or wedge segments that make up more complex features, such as junctions or edges, can be determined.

2 Signal Model

2.1 Riesz Transform

The RT is an extension of the Hilbert transform to two or more dimensions [2]. The n-th order 2D complex RT, $\mathcal{R}^n$, is a complex-valued operator that can be expressed as either a convolution in the spatial domain, or multiplication in the Fourier domain. We shall use the following definition from [7], which differs from [4], [10] only in sign changes and the position of $\mathrm{i} = \sqrt{-1}$,

$$\mathcal{R}^n f(\mathbf{z}) \quad \overset{\mathcal{F}}{\longleftrightarrow} \quad \left(\frac{u_x + \mathrm{i}u_y}{\|\mathbf{u}\|}\right)^n \hat{f}(\mathbf{u}) \tag{1}$$

where $f(\mathbf{z}) \in L_2(\mathbb{R}^2)$, $\hat{f}(\mathbf{u}) = \mathcal{F}f(\mathbf{u})$ is its Fourier transform, and $\mathbf{u} = [u_x, u_y]$. Also $\mathcal{R}^{n*} = \mathcal{R}^{-n}$ and $\mathcal{R}^0$ is the identity operator. The vector valued multi-order RT, $\boldsymbol{\mathcal{R}}^N$, maps the $-N$ to N-th order RT responses to a vector valued signal [7],

$$\boldsymbol{\mathcal{R}}^N f(\mathbf{z}) = \{\mathcal{R}^n f(\mathbf{z}) \,|\, n \in \mathbb{Z}, |n| \leq N\} \tag{2}$$

We shall refer to the response at one point as an RT vector in the rest of this paper. The higher-order RT is a unitary operator that is translation and scale invariant [2], [7], and appears as a spherical harmonic in the Fourier domain. Local signal structure with a particular rotational symmetry gives the greatest response for an RT of the same order, e.g. an 'X' junction responds most to the 4-th order RT. Therefore describing local signal structure using larger order RTs allows for more complex structures to be analysed.

2.2 2D Steerable Wavelet

The RT is also used to construct 2D steerable wavelets that are self-reversible and polar separable in the Fourier domain, [6], [7]. A 2D steerable wavelet, $s(\mathbf{z}; \theta)$, given by the weighted summation of different order RTs of an isotropic bandpass filter kernel, $p(\mathbf{z})$, is

$$s(\mathbf{z}; \theta) = \sum_{n=-N}^{N} e^{\mathrm{i}n\theta} u_n \mathcal{R}^n p(\mathbf{z}) \tag{3}$$

where θ is the orientation of the wavelet, and $\mathbf{u}$ is the weights. Let $\mathbf{f}^N(\mathbf{z}) = \boldsymbol{\mathcal{R}}^N(p * f)(\mathbf{z})$. The 2D steerable wavelet, $s_f(\mathbf{z})$, whose RT vector is the same as

the signal at $\mathbf{z} = \mathbf{0}$, i.e. $\boldsymbol{\mathcal{R}}^N s_f(\mathbf{0}) = \mathbf{f}^N(\mathbf{0})$, is given by

$$s_f(\mathbf{z}) = \frac{1}{p(\mathbf{0})} \sum_{n=-N}^{N} f_n^N \mathcal{R}^{-n} p(\mathbf{z}) \tag{4}$$

Thus a particular 2D steerable wavelet is an approximation of local signal structure up to the Nth order of symmetry. The RT is similar to the derivative operator; however, it does not change the magnitude of the filter spectrum and thus increasing the number of orders used increases the spatial extent of the filter. In contrast, 2D derivative-based steerable filters maintain spatial extent with increasing order, e.g. [11], [12]. The bandpass filter used should be smooth, with a fast rate of decay, and a large number of vanishing moments [13].

2.3 Model

Let $f(\mathbf{z}) \in L^2(\mathbb{R}^2)$ be a 2D image and $p(\mathbf{z})$ be an isotropic bandpass filter kernel chosen to restrict the analysis to a particular scale, such as a log-normal filter [14]. Assuming a local coordinate system centred on a point of interest at $\mathbf{z} = \mathbf{0}$, we propose to model the local signal structure as

$$(p * f)(\mathbf{z}) = \sum_{k=1}^{K} \alpha_k s(\mathbf{z}; \theta_k) + \epsilon(\mathbf{z}) \tag{5}$$

where $s(\mathbf{z}; \theta)$ is a real valued 2D steerable wavelet with amplitude $\alpha \in \mathbb{R}$ and orientation $\theta \in [-\pi, \pi)$, and $\epsilon(\mathbf{z})$ is a residual component. Let $\mathbf{f}^N = \boldsymbol{\mathcal{R}}^N (p*f)(\mathbf{0})$ be the signal RT vector at the point of interest, and $\mathbf{s}^N = \boldsymbol{\mathcal{R}}^N s(\mathbf{0}; 0)$ be the wavelet RT vector at orientation 0 degrees. Then

$$\mathbf{f}^N = \sum_{k=1}^{K} \alpha_k \mathbf{R}_{\theta_k} \mathbf{s}^{N\intercal} + \boldsymbol{\epsilon}^N \tag{6}$$

where $\mathbf{R}_\theta$ is the diagonal matrix $\{R^N_{\theta_{n,n}} = e^{in\theta} | n \in \mathbb{Z}, |n| \leq N\}$. A single component of the signal RT vector is therefore

$$f_n^N = s_n^N \sum_{k=1}^{K} \alpha_k \, e^{\mathrm{i}n\theta_k} + \epsilon_n^N \tag{7}$$

2.4 Super-Resolution

The problem of estimating the amplitude and orientation parameters of the model is similar to that of the super-resolution of spike trains developed in [8], [9]. This involves finding the location and amplitude of complex-valued spikes in a spike train signal from the low-frequency Fourier series components [8] even when corrupted by noise [9].

To briefly restate the problem in [8], let $x(t)$ be a signal composed of the super-position of a number of complex-valued spikes restricted to the domain $t \in [0, 2\pi)$, and $\boldsymbol{\mathcal{F}}^N$ be an operator that maps a signal to its $-N$ to Nth Fourier series coefficients. Given the Fourier series coefficients, $\mathbf{y} = \boldsymbol{\mathcal{F}}^N x(t)$ the position and amplitude of the spikes can be found by solving

$$\min_{\tilde{x}} \|\tilde{x}(t)\|_{\mathrm{TV}} \quad \text{subject to} \quad \|\boldsymbol{\mathcal{F}}^N \tilde{x}(t) - \mathbf{y}\|_{L_1} < \delta \tag{8}$$

where $\tilde{x}(t)$ is the estimated spike train, and $\|\tilde{x}(t)\|_{\mathrm{TV}}$ is the total-variation norm which selects for the solution which has the smallest number of large valued spikes. The parameter, δ, allows for noise. For an ideal spike train with no noise and $\delta = 0$, total variation minimisation will give the *exact* solution so long the wrap-around distance is greater than $4\pi/N$ for complex spikes, and $3.74\pi/N$ for real valued spikes [8]. Numerical simulations in [8] suggest that the minimum distance required may be as low as $2\pi/N$ if there are a low number of spikes compared to N. Furthermore, for real spikes all of the *same* sign, the minimum distance is practically zero. The maximum number of spikes that can be resolved is N [8]. Importantly, the super-resolution problem does not need to be made discrete. It can be solved using just the Fourier coefficients via a semi-definite program to arbitrary precision. Example MATLAB code is given in [8].

2.5 A Solution

Returning to our problem, the n-th order RT is similar to the n-th order Fourier series component of the angular portion of the signal spectrum, and eq. (7) is equivalent to the Fourier series of a spike train weighted by $\mathbf{s}^N$. Let

$$g_n^N = f_n^N / s_n^N \tag{9}$$

$$r_n^N = \sum_{k=1}^{K} \alpha_k e^{\mathrm{i}n\theta_k} \tag{10}$$

where $|n| \leq N$. Note that $\mathbf{g}^N$ is the signal RT vector normalised by the 2D wavelet coefficients; this division is the crucial step that converts the problem from a super-position of wavelets to a super-position of spikes. The RT vector $\mathbf{r}^N$ corresponds to the desired solution. According to the super-resolution theory we may then solve

$$\min_{\boldsymbol{\alpha}} \|\boldsymbol{\alpha}\|_{\mathrm{TV}} \text{ subject to } \|\mathbf{r}^N - \mathbf{g}^N\| < \delta_\epsilon \tag{11}$$

to obtain the amplitudes and orientations of the component wavelet. Since the maximum number of spikes that can be recovered is N, we have $K \leq N$.

We have assumed the signal can be reasonably modelled by our choice of wavelet. If it cannot, there is no guarantee the signal will be angularly band-limited in the same way the wavelet is. Thus if for some n, s_n^N is small, g_n^N can be potentially quite large and have a disproportionate effect on the results. The wavelets we shall consider have coefficients with unity magnitude however, i.e. $|s_n^N| = 1$. If no solution is found, δ_ϵ, should be increased.

3 Feature Types

The main application of this work is to parametrise image features that are made up of a particular feature component overlaid at different amplitudes and orientations. For example, finding the amplitude and orientation of line segments that make up a 'Y' junction, or the angle of the edges that make up a corner. A junction or corner feature located at the point of interest, $\mathbf{z} = \mathbf{0}$, of an image signal $f(\mathbf{z})$ can be described by

$$f(\mathbf{z}) = \sum_{k=1}^{K} \alpha_k t(\mathbf{z}; \theta_k) \tag{12}$$

where $t(\mathbf{z})$ is the feature component, such as a line segment. If $s_{\mathrm{t}}(\mathbf{z}; 0)$ is the 2D steerable wavelet approximation of $(p * t)(\mathbf{z})$, then we have

$$(p * f)(\mathbf{z}) = \sum_{k=1}^{K} \alpha_k s_{\mathrm{t}}(\mathbf{z}; \theta_k) \tag{13}$$

Using the super-resolution method the amplitude and orientation of the wavelets can be found, and thus so can the amplitude and orientation of the underlying component $t(\mathbf{z})$. We shall consider features composed of line segments and wedge segments.

3.1 Line Types

We define a line segment as a line radiating from a point with a constant amplitude and orientation. Local features such as 'Y' or 'X' junctions are composed of multiple line segments.

An idealised line segment radiating from $\mathbf{z} = \mathbf{0}$ can be described in polar coordinates, $\mathbf{z} = [r\cos\phi, r\sin\phi]$, by the function

$$t_{\mathrm{line}}(r, \phi; \theta) = \alpha \frac{\delta(\phi - \theta)}{r} \tag{14}$$

where α is the amplitude and θ is the orientation. Modifying our previous results in [10] to account for the different form of the RT used in this paper, the n-th order RT at origin is

$$\mathcal{R}^n(p * t_{\mathrm{line}})(\mathbf{0}) = (-\mathrm{i})^{|n|} \alpha e^{\mathrm{i}n\theta} \int_0^\infty \hat{p}(w) dw \tag{15}$$

where $\hat{p}(w)$ is the Fourier transform of the bandpass filter expressed in polar coordinates, $w = \|\mathbf{u}\|$. The corresponding wavelet decomposition is

$$s_{\mathrm{line}}(\mathbf{z}; \theta) = \frac{1}{p(\mathbf{z})} \sum_{n=-N}^{N} \mathcal{R}^n(p * t_{\mathrm{line}})(\mathbf{0}) \cdot \mathcal{R}^{-n} p(\mathbf{z}) \tag{16}$$

$$= \frac{\alpha C}{p(\mathbf{0})} \sum_{n=-N}^{N} e^{\mathrm{i}n\theta} \mathcal{R}^{-n} p(\mathbf{z}) \tag{17}$$

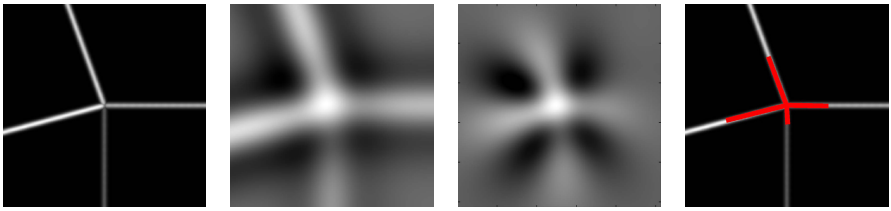

(a) Feature, $f(\mathbf{z})$ **(b)** $(p * f)(\mathbf{z})$ **(c)** $s_f(\mathbf{z})$ **(d)** Solution

Fig. 1. Estimating the amplitude and orientation of a line feature (a). Bandpassed signal shown in (b) with wavelet approximation (c). Amplitude (length of line) and orientation solution shown in (d).

where C is a constant dependent on the filter used. Finally, the normalised RT vector we shall use when solving for a line feature is

$$\mathbf{t}^N_{\text{line}} = \{(-\mathrm{i})^{|n|} \,|\, n \in \mathbb{Z}, |n| \leq N\} \tag{18}$$

3.2 Edge Types

Consider a feature composed of wedge segments, such as chequerboard or a corner where solid planes meet. A wedge segment with edge angles θ_1, θ_2 may be represented in polar coordinates by

$$t_{\text{wedge}}(r, \phi; \theta_1, \theta_2) = \begin{cases} \alpha & \text{where } \phi \in [\theta_1, \theta_2) \\ 0 & \text{otherwise} \end{cases} \tag{19}$$

Solving this is a little more difficult. We begin by considering the RT response of the wedge segment without the bandpass filter, using the spatial expression for the RT in [7],

$$\begin{aligned} \mathcal{R}^n t_{\text{wedge}}(\mathbf{0}) &= \langle (\mathcal{R}^n \delta)(-\mathbf{z}), t_{\text{wedge}}(\mathbf{z}) \rangle & (20) \\ &= \int_0^\infty \int_0^{2\pi} \frac{n\mathrm{i}^{|n|}}{2\pi} \frac{e^{\mathrm{i}n(\phi-\pi)}}{r^2} t_{\text{wedge}} \, d\theta \, r dr & (21) \\ &= n\,\mathrm{i}^{|n|}(-1)^n \frac{\alpha}{2\pi} \int_0^\infty \int_{\theta_1}^{\theta_2} \frac{e^{\mathrm{i}n\phi}}{r^2} \, d\theta \, r dr & (22) \\ &= (-\mathrm{i})^{|n+1|} \frac{\alpha}{2\pi} (e^{\mathrm{i}n\theta_2} - e^{\mathrm{i}n\theta_1}) \int_0^\infty \frac{1}{r} dr & (23) \\ &= (-\mathrm{i})^{|n+1|} \frac{\alpha}{2\pi} (e^{\mathrm{i}n\theta_2} - e^{\mathrm{i}n\theta_1}) \lim_{a \to 0} \int_a^\infty \frac{1}{r} dr & (24) \end{aligned}$$

The limit in the above equation tends to infinity, however the main result is that the magnitude of the response has the same bounds regardless of RT order, n. For example, the magnitude of the response of the 1st order kernel to an edge

($\boldsymbol{\theta} = [0, \pi]$) is the same as a 2nd order kernel to a corner ($\boldsymbol{\theta} = [0, \pi/2]$). If the signal is bandpassed using a filter kernel that decays to zero fast enough, then we may still write

$$\mathcal{R}^n(p * t_{\text{wedge}})(\mathbf{0}) = (-\mathrm{i})^{|n+1|} D(e^{\mathrm{i}n\theta_2} - e^{\mathrm{i}n\theta_1}) \tag{25}$$

where D is a constant dependent on the filter used. The corresponding wavelet is given by

$$s_{\text{wedge}}(\mathbf{z}; \theta_1, \theta_2) = \frac{D}{p(\mathbf{0})} \sum_{n=-N}^{N} (-\mathrm{i})^{|n+1|} (e^{\mathrm{i}n\theta_2} - e^{\mathrm{i}n\theta_1}) \mathcal{R}^{-n} p(\mathbf{z}) \tag{26}$$

Rewriting as the sum of two wavelets, s_{edge},

$$s_{\text{wedge}}(\mathbf{z}; \theta_1, \theta_2) = s_{\text{edge}}(\mathbf{z}; \theta_2) - s_{\text{edge}}(\mathbf{z}; \theta_1) \tag{27}$$

$$\text{where} \quad s_{\text{edge}}(\mathbf{z}; \theta) = \frac{D}{p(\mathbf{0})} \sum_{n=-N}^{N} (-\mathrm{i})^{|n+1|} e^{\mathrm{i}n\theta} \mathcal{R}^{-n} p(\mathbf{z}) \tag{28}$$

we obtain the normalised edge RT vector,

$$\mathbf{t}_{\text{edge}}^N = \{(-\mathrm{i})^{|n+1|} \mid n \in \mathbb{Z}, |n| \leq N\} \tag{29}$$

which is the component that will be used to analyse edge features such as corners.

3.3 Smoothed Features

Line or edge features often appear smoothed in images. Let $g(\mathbf{z})$ be an band-limited isotropic smoothing kernel, such as a Gaussian, applied to our idealised line or edge feature, e.g. $(g * f)(\mathbf{z})$. Substituting $p_g(\mathbf{z}) = (p * g)(\mathbf{z})$ for the wavelet generating kernel, $p(\mathbf{z})$, in the previous two sections yields the same normalised line and edge RT vectors. The super-resolution method therefore remains the same.

3.4 Procedure

A general procedure resolving a line or edge feature is as follows:

1. Choose bandpass filter and maximum order, N, of RTs to be used.
2. Calculate RT vector at point of interest using eq. (2).
3. Determine whether local structure is a line or edge type. One method is compare the 0-th order RT response to that of the other orders. If it is around the same magnitude it is a line type, if it is closer to 0 it is an edge type.
4. Choose RT vector corresponding to the type, $\mathbf{t}_{\text{line}}(\mathbf{z})$ for positive lines, $-\mathbf{t}_{\text{line}}(\mathbf{z})$ for negative lines, $\mathbf{t}_{\text{edge}}(\mathbf{z})$ for edge types.
5. Solve eq.(11) using the super-resolution method to get the relative amplitudes and orientations. Increase δ_ϵ and re-evaluate if no solution is returned.

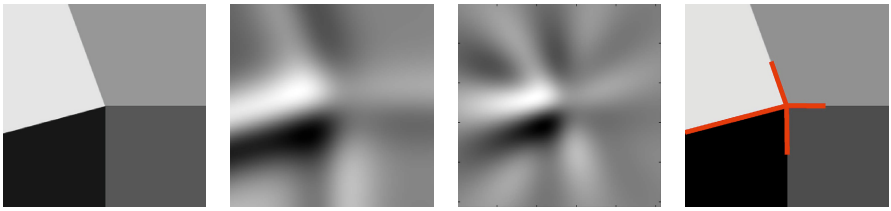

(a) Feature, $f(\mathbf{z})$ **(b)** $(p * f)(\mathbf{z})$ **(c)** $s_f(\mathbf{z})$ **(d)** Solution

Fig. 2. Estimating the amplitude and orientation of an edge feature (a). Bandpassed signal shown in (b) with wavelet approximation (c). Amplitude (length of line) and orientation solution shown in (d).

From the solution, one can classify the feature according to the number of components with amplitude above a certain threshold. Figures 1 and 2 show the wavelet approximation and super-resolution solution for a line and edge feature, respectively.

4 Experiments

4.1 Minimum Distance

The minimum distance condition needed for accurate super-resolution requires the segments of a line or edge feature to be separated by a given angle, which depends on the maximum order RT used. The minimum angle required for an exact solution was numerically evaluated for different numbers of segments. An ideal signal comprised of from three to five real valued spikes (segments) was solved from its Fourier series coefficients (RTs), using the super-resolution method with $N \in [2, 9]$. The minimum distance between adjacent spikes of the same sign, and of the opposite sign, that gave an accurate solution is shown in Figure 3. Generally for all N, the minimum distance required between spikes of the same sign was less than 0.1 radians, even if the signal contained opposite sign spikes. For opposite sign spikes, a minimum distance of π/N radians was needed. Knowing the expected minimum angle between segments in a line or edge feature can therefore guide the maximum order RT required.

4.2 Running Time

Average running time to calculate a solution in MATLAB, using one core of a 3GHz Core2 Quad Intel processor, ranged approximately linearly from 0.56s ($N = 2$) to 1.04s ($N = 10$).

4.3 Noise Sensitivity

A 'T' junction image, $f(\mathbf{z})$, consisting of 1-pixel wide line segments orientated at 0, 90 and 180 degrees was corrupted with varying levels of Gaussian noise.

The angle and orientation of the lines were found using our method with $\delta_\epsilon = 0.1 \times |\mathbf{f}^N|$, $N \in [2, 10]$, and a log-normal filter of wavelength 32 pixels and $\sigma = 0.65$. The average error is shown in Figure 4 (a) and (b). Figure 4 (c) shows the same experiment but with $N = 5$, and δ_ϵ ranging from 0.1 to $0.7 \times \|\mathbf{f}^N\|$. Increasing N decreases the amplitude and orientation error at the expense of longer computation time. For low noise values, increasing δ_ϵ increases the amplitude and orientation errors proportionally. However, if N is also increased these errors are reduced (not shown). In contrast, the percentage of solutions correctly classified as having three line segments (above 10% of maximum amplitude) improved with increasing δ_ϵ, because a larger value reduces the need for spurious components to compensate for noise.

4.4 Comparison

A recent method to estimate the orientation of line and edge segments is multi-steerable matched filters (MSMF) [12]. We tested the performance of our method (log-normal filter, $\sigma = 0.65$, wavelength $= [19, 10]$ for $N = [6, 12]$, respectively) against MSMFs (maximum derivative order of 28) for orientation estimation of a two line-segment feature. Orientation from the two maxima of the angular response of the component line-segment 2D steerable wavelet was also compared. The feature was constructed as two one-pixel wide line segments smoothed using a Gaussian kernel ($\sigma = 1.25$) with added Gaussian noise ($\sigma = 1$). Figure 5 shows the results. Our method using only six RT orders performs similarly to MSMFs using 28 derivative orders, and performs better for 12 RT orders. For small differences in line-segment orientation, super-resolution gives less error than simply rotating the line-segment wavelet and finding the local maxima of the response. This is because super-resolution can often resolve two line segments when there is only one peak in the angular response.

4.5 Example Images

Figure 6 shows the analysis of bee-wing vein junctions found using our method. Amplitude and orientation of the line segments were found using the negative line-segment RT vector ($-\mathbf{t}_{\text{line}}$, $N = 7$, $\delta_\epsilon = 0.3 \times |\mathrm{f}^N|$) using a log-normal filter with wavelength 16 and $\sigma = 0.65$. Each junction was classified according to the number of component line-segment wavelets with amplitude above 0.15 times the maximum amplitude.

A few of the junctions are misclassified, highlighting a challenge with practical application. Firstly, our signal model assumes that the line or edges of the image feature are radiating from the centre of the feature; therefore, the locations chosen must be as close to the centre of the feature as possible. Secondly, as the signal model only uses one particular component, i.e. line segment or edge segment, the solution given by the super-resolution method may return extra components to compensate for other types of structures present.

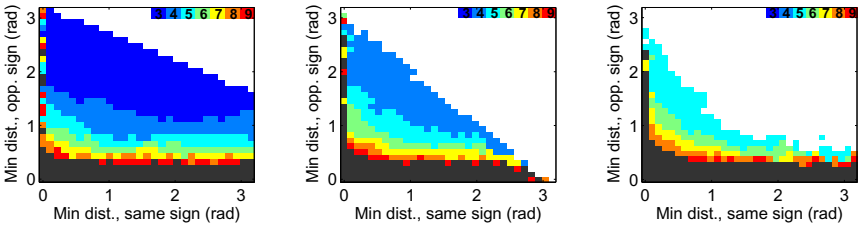

(a) 3 spikes **(b)** 4 spikes **(c)** 5 spikes

Fig. 3. Minimum distances between same sign spikes, and opposite sign spikes, for three to five spikes solved with $N \in [3, 9]$. Coloured areas indicate values where the solution was accurate for a particular order N. Areas for large N include that of smaller N. Grey areas indicate no accurate solution found for all evaluated orders.

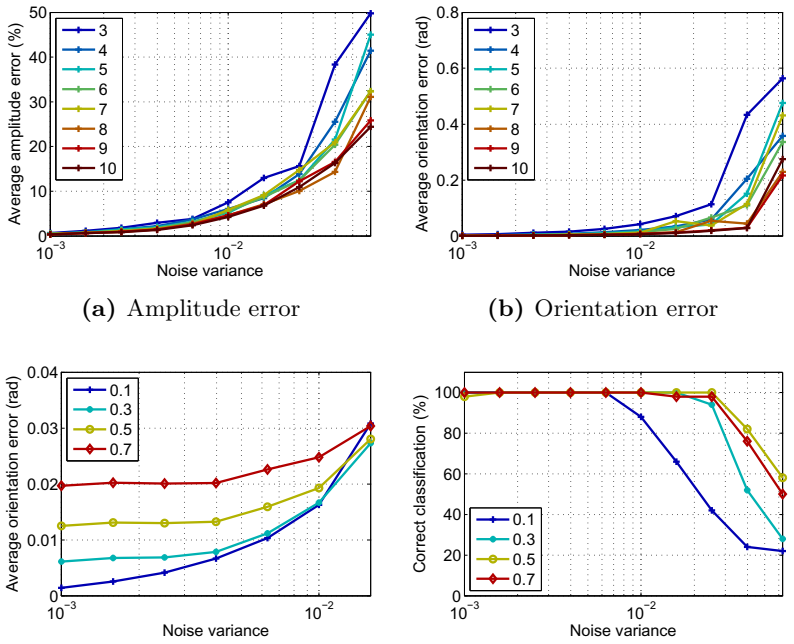

(a) Amplitude error **(b)** Orientation error

(c) Effect of δ_ϵ **(d)** Classification Rate

Fig. 4. Effects of noise, order (N) and δ_ϵ: Amplitude error (a) and orientation error (b) vs increasing noise for different N (coloured lines) with $\delta_\epsilon = 0.1 \times |\mathbf{f}^N|$; amplitude (solid line) and orientation (dashed line) error (c) and classification rate (d) vs noise for different δ_ϵ (coloured lines) with $N = 5$

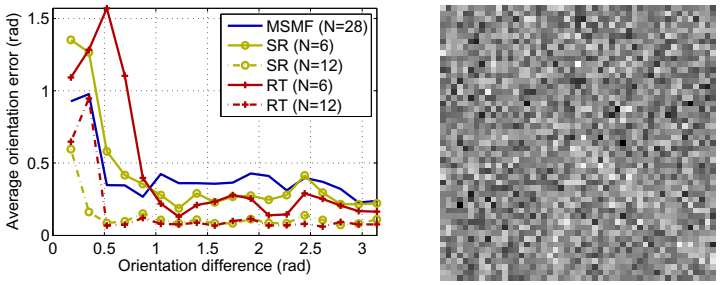

(a) Results **(b)** Example Test Image

Fig. 5. Our method (SR) compared to multi-steerable matched filters (MSMF), and local maxima of the wavelet angular response (RT), for estimating the orientations of two line segments (a), with example shown in (b)

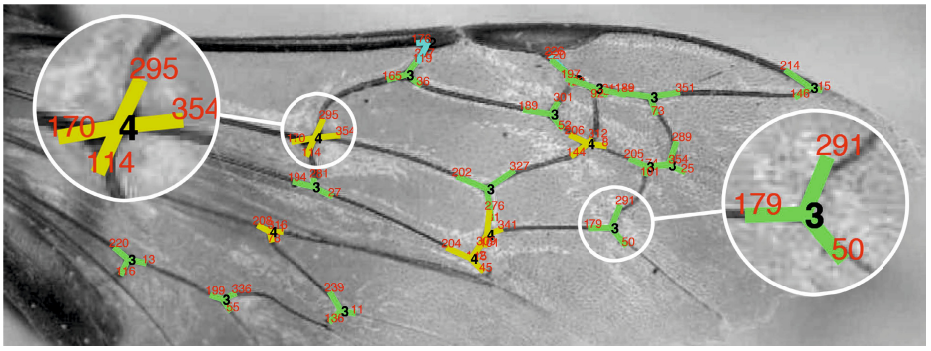

Fig. 6. Bee-wing vein junctions classified by number of line segments (black number). Lines indicate amplitude and orientation of line segments, with the angle shown in degrees (red numbers).

5 Conclusion

In this paper we have presented a novel method of representing local image structure as the superposition of either a line- or edge-type 2D steerable wavelet at multiple amplitudes and orientations. This provides a description of local image structure with rich geometric information, enabling junction or corner features to be classified by the number and position of their components. Steerable wavelets are used because they are generated using RTs, which maintain the scale of analysis when the order, N, is increased. In our experiments, the method compares favourably with multi-steerable matched filters, which use derivatives, for estimating line orientation.

Estimating the amplitudes and orientations using the super-resolution method allows for arbitrary accuracy without needing to discretise the problem, as would

be necessary if solving using linear programming. For an ideal feature with any number of line or edge segments the solution will be exact, regardless of N, provided the minimum distance criteria is met. In the presence of noise, increasing N decreases error. Representing local image structure using 2D steerable wavelets with non-unitary RT vectors is the subject of future work.

References

1. Newell, A., Griffin, L.: Natural Image Character Recognition Using Oriented Basic Image Features. In: Proc. Int. Conf. Digital Image Computing Techniques and Applications, pp. 191–196 (December 2011)
2. Felsberg, M., Sommer, G.: The monogenic signal. IEEE Trans. Signal Process. 49(12), 3136–3144 (2001)
3. Zang, D., Sommer, G.: The Monogenic Curvature Scale-Space. In: Reulke, R., Eckardt, U., Flach, B., Knauer, U., Polthier, K. (eds.) IWCIA 2006. LNCS, vol. 4040, pp. 320–332. Springer, Heidelberg (2006)
4. Wietzke, L., Sommer, G.: The Signal Multi-Vector. J. Math. Imaging and Vision 37(2), 132–150 (2010)
5. Fleischmann, O., Wietzke, L., Sommer, G.: Image Analysis by Conformal Embedding. J. Math. Imaging and Vision 40(3), 305–325 (2011)
6. Unser, M., Van De Ville, D.: Wavelet steerability and the higher-order Riesz transform. IEEE Trans. Image Process. 19(3), 636–652 (2010)
7. Unser, M., Chenouard, N.: A unifying parametric framework for 2D steerable wavelet transforms. SIAM J. Imaging Sci. 6(1), 102–135 (2012)
8. Candes, E., Fernandez-Granda, C.: Towards a mathematical theory of super-resolution. arXiv preprint arXiv:1203.5871 (2012)
9. Candes, E., Fernandez-Granda, C.: Super-resolution from noisy data. arXiv preprint arXiv:1211.0290 (2012)
10. Marchant, R., Jackway, P.: Feature detection from the maximal response to a spherical quadrature filter set. In: Proc. Int. Conf. Digital Image Computing Techniques and Applications (December 2012)
11. Freeman, W.T., Adelson, E.H.: The design and use of steerable filters. IEEE Trans. Pattern Anal. Mach. Intell. 13(9), 891–906 (1991)
12. Mühlich, M., Friedrich, D., Aach, T.: Design and Implementation of Multisteerable Matched Filters. IEEE Trans. Pattern Anal. Mach. Intell. 34(2), 279–291 (2012)
13. Ward, J., Chaudhury, K., Unser, M.: Decay properties of Riesz transforms and steerable wavelets. arXiv preprint arXiv:1301.2525 (2013)
14. Boukerroui, D., Noble, J., Brady, M.: On the Choice of Band-Pass Quadrature Filters. J. Math. Imaging and Vision 21(1), 53–80 (2004)